Progress In Electromagnetics Research M, Vol. 57, 11–24, 2017

Analysis of Multi-Resonance Characteristics in Suspended Ring Antenna Applicable for IoT/WSN

Sraddhanjali Mohapatra, Debaprasad Barad*, and Subhrakanta Behera

Abstract—In this work, the multi-resonance behavior of a suspended ring antenna structure with a single port has been investigated. Introduction of symmetrical slots at each arm of the ring structure enables quad-band operation. The antenna yields good impedance matching at 3.4 GHz, 4.5 GHz, 5.8 GHz and 7.5 GHz with considerably high gain response up to 6 dBi. Maintaining suitable air height from the ground plane enhances the bandwidth up to 12%. This compact antenna shows bandwidths of 130 MHz, 360 MHz, 850 MHz, and 380 MHz, respectively. Each resonance claims an efficient use in next generation wireless communication within S-band and C-band radio links extensively and also applicable in WSNs/IoTs which requires a multi-functional antenna system. Theoretical analysis of the proposed antenna is investigated with the equivalent lumped circuit. The antenna element is excited using separate feed patch alongside of the ring. The antenna exhibits TM_{10}, TM_{01}, TM_{11} excitation modes at different resonances. The said antenna is implemented on an FR4 substrate with dielectric constant of 4.4, substrate thickness of $h = 1.56$ mm and loss tangent of $\tan\delta = 0.02$. The antenna is designed with physical dimensions of $18 \times 18 \times 7.56\,\text{mm}^3$ which claims its compactness.

1. INTRODUCTION

Recently, many researchers have focused on the development of an efficient multi-functional wireless communication technology, which can map the bigger complex communication to a compact transparent one. This mapping involves multi-operational wireless devices with multi-tasking capabilities using a single compact device [1]. Practicability of this requirement is well realized using a novel compact antenna, which can perform over multiple operational RF bands with better polarization characteristics. Multi-band design approach will be helpful for incorporating more than one band of frequency simultaneously, which will be positively applicable to RF wireless communications [2]. It has been reported that a compact full multi-functional antenna is well implemented by considering printed type antenna [3]. The antennas having wide-bandwidth, high gain, multiple operational bands, and enhanced polarization characteristics are inevitable for configuring wireless communication system [4]. Apart from compactness, the printed antennas are considered as the most suitable choice due to its low-cost design, ease of fabrication, ease of integration into MMIC design, extremely light weight, and low-profile design [5]. The printed antenna design realizes widespread application in ISM band including applications in Bluetooth, GPS, ZigBee, RFID, WLAN, RADAR, Wi-MAX, HYPERLAN, WSN etc. [6]. It has been observed that the multiple bands of operation are realized from complex miniaturization [7], ground modification [8], stacked ring [9], annular ring [10], etc., but these designs are somewhat difficult for extended analysis and optimization, and it also takes more computational time.

This multi-band concept reduces the estimated cost; minimize the requirement of number of transceivers, base stations, terminals, etc. Many researchers are doing research in the mentioned field, but the quad-band operation cannot be succeeded till date. Since last decade, rigorous research has been

Received 24 February 2017, Accepted 27 April 2017, Scheduled 14 May 2017
* Corresponding author: Debaprasad Barad (deba7482@gmail.com).
The authors are with School of Electronics Engineering, KIIT University, Bhubaneswar-24, India.

carried out for developing highly efficient multi-functional antennas and its utilization in smart sensor network [11]. Although numerous designs are proposed for multi-band operation, the system requirement was not achieved successfully. Likewise, the designed antennas are unable to confirm the substantial characteristics. In fact, the designs have fewer bands like dual-band, poor impedance matching, in some cases, worst polarization characteristics and limited gain [12]. In reference to the recent research works on high-efficient antenna design for wireless sensor node in [13], the antenna comprises a dual-band with miserable impedance matching. However, this work conquered the frustration realized and wrapped up better impedance bandwidth and improved polarization characteristics with high response.

With each passing day, the wireless technology adopts multi-functional compact transceiver in the communication terminals for reducing the costs and complexity [14]. On top of the technology Internet of Things (IoT) is a modern trend in wireless communication, which was matured laterally with WSNs. The multi-tasking wireless communication technology has a major role in IoT, notably WSNs proliferate a great demand in industrial application, in which small, reasonable cost, low powered WSN sensor realizes the smallest and smartest IoT configuration. Application of this WSN structure can identify and meet the market trends of future technology as reported in a white paper [15]. Also, it has been reported that the practical implementation of IoT/WSN structure requires efficient smart sensor terminals with multi-tasking communication transceivers, in which the transceivers are the practical representation of high-efficiency antenna capable of handling multi-signal transmission with an improved band of operation, enhanced gain response, reasonably small size and economically low cost, etc. In this study, a novel suspended microstrip patch antenna (MPA) is suggested which fulfills the requirement of the IoT/WSN standards as discussed above. The communication system can be remodeled to achieve multi-signal transmission and reception in sensor networking.

This paper investigates the multi-band operation from a square ring structure designed in a single FR4 substrate without ground modification and complex structure. A single port analysis of a novel square ring structure with rectangular slots at each boundary has been studied extensively. The antenna is excited using EM coupling from the same layer. This specified structure resonates at multiple bands of 3.4 GHz, 4.5 GHz, 5.8 GHz and 7.5 GHz with comparatively better reflection coefficient, impedance bandwidth, gain response, etc. The resonating bands 3.4 GHz and 5.8 GHz are found widely used in Wi-MAX communication [16], and 4.5 GHz is used for fixed military mobile communication by US & NATO [17]. Also this band is used for optimizing the throughput speed about 10 Gbps in below 6 GHz 5G communication as suggested by Youell [18]. The 7.5 GHz band is used for the optimization of regional and ANS systems as notified by ITU-R [19]. In addition, these resonating bands are universally suitable for S-band and C-band microwave communication links in satellite/RADAR communication. Also, the resonating bands of this antenna propose its application in wireless sensor network for resolving fixed security issues.

2. DESIGN AND ANALYSIS OF ANTENNA STRUCTURE

2.1. Antenna Design

The suggested multi-band linearly polarized antenna system is designed on a single dielectric substrate, followed by a single port analysis. This antenna structure was implemented on an FR4 substrate of relative permittivity $\varepsilon_r = 4.4$, substrate thickness $h_s = 1.56\,\text{mm}$, and loss tangent $\tan\delta = 0.02$. The printed antenna investigated in this study is a multi-layer structure, wherein the antenna patch is placed at the top of the dielectric layer above the ground plane with an air height of $h_a = 6\,\text{mm}$ followed by the substrate thickness of h_s. The proposed antenna structure is of comparatively less volume of $18 \times 18 \times 7.56\,\text{mm}^3$, which is convenient for configuring a multi-standard, multi-functional microwave communication system. A nearly square patch of $L_p \times W_p$ is considered as the antenna radiator patch. Later this patch is altered to a ring structure intended for multi-signal propagation. This modified radiator patch is excited using capacitive coupling due to a feed patch of $L_f \times W_f$ present alongside. A separate patch is implemented rather than direct feeding to the radiator patch to avert the variation in resonating bands. A $50\,\Omega$ coax probe is inserted into the substrate from the ground plane through an SMA connecter united behind the ground plane. The cross-sectional view of the suggested antenna structure is shown in Figure 1(a).

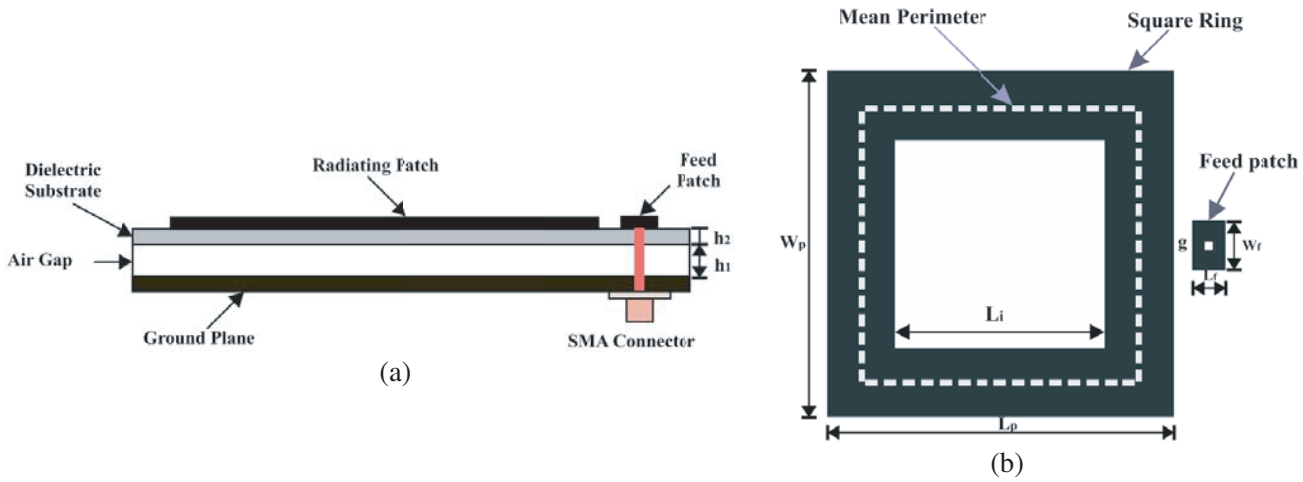

Figure 1. Design structure of the suggested antenna. (a) Cross view of the antenna structure. (b) Top view of the antenna geometry.

A square slot of $L_i = 8\,\text{mm}$ was dug at the center ($x = 0$, $y = 0$) on the conventional antenna geometry, which accomplishes the ring formation. The ring structure of the antenna radiator patch is favorable for dual-band operation at 4.1 GHz and 5.8 GHz, because of the discontinuities developed by the patch and the later added slot. As observed, in a ring structure the resonant frequencies are primarily determined by considering the mean perimeter (Mp) of the ring marked in a dotted line, in which the lower order resonance is determined by considering the outer patch length ($l_{p(eff.)}$) and the inner ring length (L_i) [20–22]. However, this modified antenna geometry exhibits superior impedance matching at both of the resonances with improved impedance bandwidth of 500 MHz at 4.1 GHz and around 1 GHz of wideband operation at the higher order resonance 5.8 GHz. Theoretical analysis of the presented antenna patch (Figure 1(b)) may be carried out through lumped circuit analysis. The substantial dimensions of the conventional antenna were determined using Equations (1) and (2).

$$L_{p(eff.)} = \frac{c}{f_{rp1}} \times \frac{k}{\varepsilon_{eff.}} \tag{1}$$

$$L_i = \frac{c}{f_{rp2}} \times \frac{k}{\varepsilon_{eff.}} \tag{2}$$

The calculation of the patch dimension primarily depends on the design frequency of the Microstrip patch antenna (MPA). The layout of the conventional antenna geometry is shown in Figure 1(b). The square ring structure exhibits dual-wideband operation at the specific frequency band, where the second/higher order resonance is caused by the inner ring length, and the outer ring length is responsible for lower order resonance. The designed antenna geometry shown in Figure 1(b) can be reconfigured for wideband operation by optimizing the dimensions of square slot (L_i). The optimized dimension of the proposed antenna is mentioned in Table 1.

The constant $k\,(= 0.25)$ is considered here for properly setting the design equation. The design Equations (1) and (2) are derived from [5]. The effective dielectric constant ($\varepsilon_{eff.}$) of the suggested suspended antenna is determined using the equation given below; the calculation of $\varepsilon_{eff.}$ parameter involves w/h ratio. There is a different equation derived for $w/h < 1$ and $w/h > 1$. But as per our proposed antenna structure, corresponding equation of $\varepsilon_{eff.}$ is cited here,

$$\varepsilon_{eff.} = \frac{\varepsilon_r\,(1 + (h_a/h_s))}{(1 + \varepsilon_r\,(h_a/h_s))} \tag{3}$$

Table 1. Dimension for proposed multi-band antenna.

Parameter	Value
Length of the radiator patch (L_p)	15.5 mm
Width of the radiator patch ($W_p \cong L_p$)	16.4 mm
Length of the feed strip (L_f)	0.6 mm
Width of the feed strip (W_f)	1.2 mm
Separation gap between feed strip patch from radiator patch (g)	0.5 mm
Length of the square slot (L_i)	8 mm
Air gap between substrate and ground plane ($h_a = h_1$)	6 mm
Thickness of the substrate ($h_s = h_2$)	1.56 mm
Relative dielectric constant of the substrate (ε_r)	4.4

2.2. Configuration and Discussion of Multi-Band Antenna

The designed dual-band ring structure was taken into consideration for realizing multi-band operation with improved impedance bandwidth and better gain response. The ring structure of the antenna geometry is miniaturized by introducing rectangular slots. The rectangular slots of dimensions $L_s \times W_s$ are dug at each side of the ring, where the slots are aligned to the center of the ring in line with the mean perimeter marked with a dotted line as demonstrated in Figure 1(b) and also Figure 2(b).

The ring structure of the antenna geometry is miniaturized by introducing rectangular slots. The newly created slot increases the number of discontinuities in the antenna radiator patch. As discussed earlier, higher number of discontinuities will introduce extra edge capacitance. This capacitance influences multi-resonance behavior in the antenna characteristics. Although the slots are introduced at the four arms of the square ring as shown in Figure 2(a), the multi-resonance operation is not achieved. The $|S_{11}|$ characteristic of this designed antenna gives dual-band operation, even if slots are introduced. Later, the dimensions of the newly introduced slots are increased, wherein the desired multi-resonance characteristics are obtained. In fact, the introduction of a slot centering to the mean perimeter line splits the ring, and the modified geometry can have analyzed as a dual-ring structure [23]. The modified final antenna geometry with slots at boundary is presented in Figure 2(b), which concludes multi-resonance characteristics with enhanced impedance bandwidth and reflection coefficient at four different frequency bands 3.4 GHz, 4.5 GHz, 5.8 GHz and 7.5 GHz. In addition to this, the narrow band characteristics of the MPAs are conquered, and the optimized result exhibits wideband operation as demonstrated in Figure 2(c). This figure also distinguishes the $|S_{11}|$ characteristics using different antenna configurations, without slotted boundary and with slotted boundary. Initially, a symmetrical rectangular slot of $L_s = 1$mm and $W_s = 6$ mm was dug, and later the slot is periodically optimized with different $L_s \times W_s$ valus, demonstrated in Figure 2(d). However, the slots having dimensions of $L_s = 1$ mm and $W_s = 12$ mm give superior return loss characteristics. Although the observation shows that the slot with $L_s = 1.1$ and $W_s = 12$ mm shows enhanced $|S_{11}|$ parameter, it was not considered as it fails to give symmetrical slotted structure. The multi-resonance behavior of the suggested antenna can be realized by deriving separate equation for each resonant frequency.

2.3. Theoretical Analysis of the Suspended Microstrip Patch

The theoretical study of the conventional ring structure may be analyzed using a lumped circuit equivalent. Stage wise analysis of lumped circuit equivalent is accomplished in Figure 3. Computation of input impedance Z_{in} involves the corresponding inductance and capacitance values of each element. Although there is an existence of resistance in each element, this resistance value may be treated as negligible during high frequency analysis. Z_{in} is analyzed along with the excitation direction, wherein the probe is replaced as an inductive load (L_{probe}). The rest of the patches are replaced as inductive and or capacitive load. The separation gap between the feed patch and radiator patch is represented by an equivalent capacitance value.

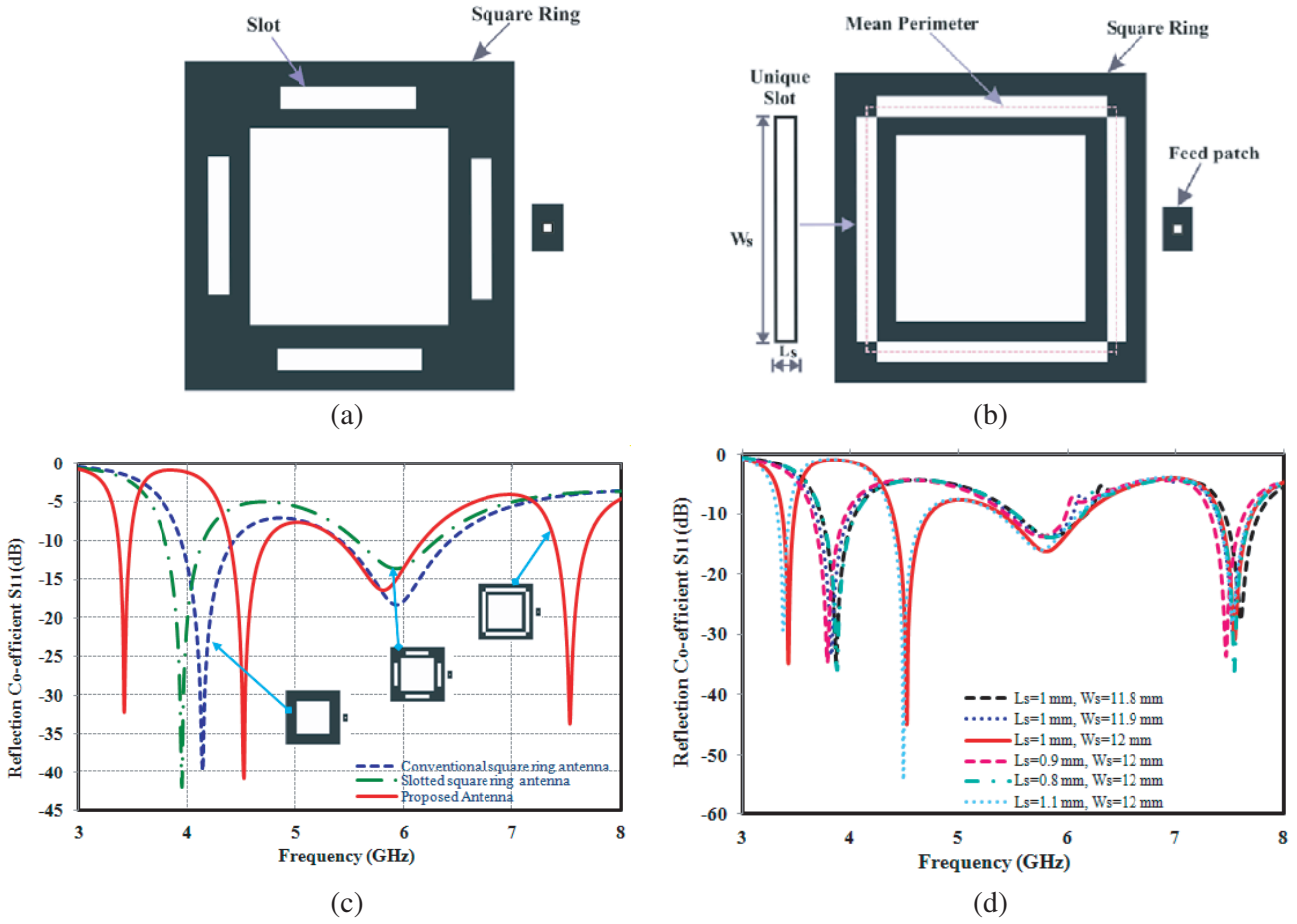

Figure 2. (a) Suspended antenna patch with slotted ring. (b) Proposed antenna geometry with optimized slot for quad-band operation. (c) Iterative observation of $|S_{11}|$ characteristic without slot, with slots and final antenna patch. (d) Periodic optimization of $|S_{11}|$characteristic using different L_s and W_s.

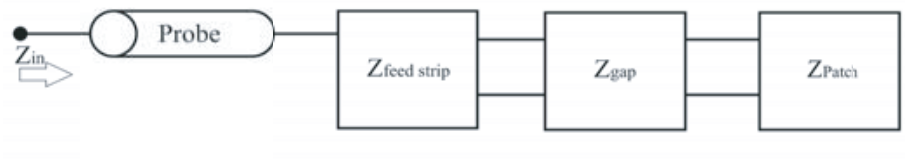

Figure 3. Simplified lumped circuit equivalent of the suspended ring antenna.

The equivalent input impedance Z_{in} can be calculated using Equation (4), by considering the impedance values of each element as depicted in Figure 3. The impedance value of each element can be calculated using the individual reactance value of the corresponding capacitor or inductor as presented in Figures 4 and 5, in which $Z_{\text{feed strip}}$ is the impedance due to feed patch, Z_{gap} due to the separation gap, and Z_{patch} due to the ring element. This Z_{patch} is calculated by considering the equivalent ring impedance $Z_{\text{ring(outer)}}$ parallel with $Z_{\text{ring(inner)}}$ with an effective capacitance arises due to non-metallic slot.

$$Z_{in} = j\omega L_{probe} + \left(\frac{1}{Z_{feedstrip}} + \frac{1}{Z_{gap}} + \frac{1}{Z_{patch}}\right)^{-1} \tag{4}$$

The designed antenna patch on the dielectric layer is analyzed for multi-resonance operation, and the

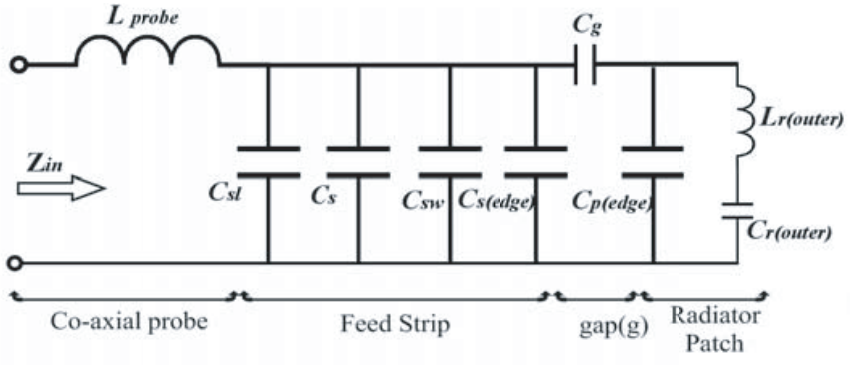

Figure 4. Lumped circuit equivalent of the suspended antenna with single ring (Figure 1(b)).

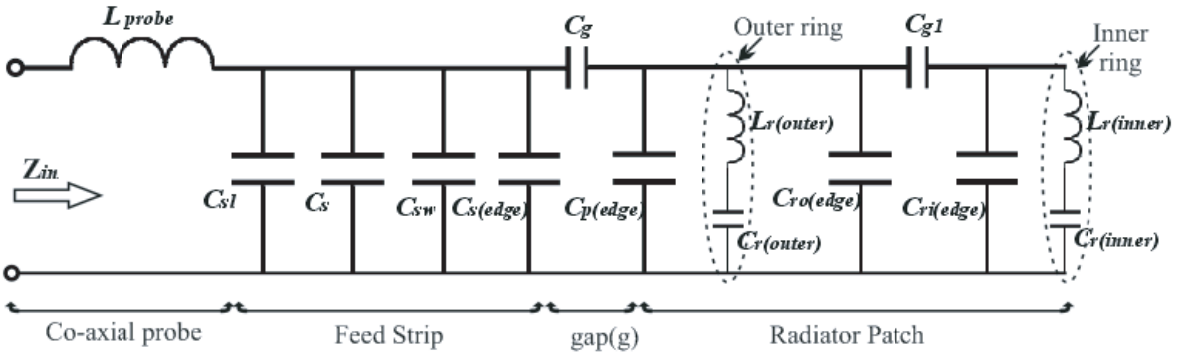

Figure 5. Lumped circuit equivalent of the suspended antenna with slotted ring (Figure 2(b)).

electrical equivalent circuit is verified using EDA software. As discussed in the above section, single ring configuration makes a loop whose impedance characteristics can be represented as an LC lumped circuit equivalent (Figure 4). This lumped model is typically a parallel tuned circuit operating in the fundamental modes of the corresponding antenna patch. However, the equivalent circuit for extremely high frequency operation can be placed using an inductor and a capacitor. The present configuration can be analyzed as an edge fed microstrip antenna having an edge capacitance of c_{edge} coupled with the equivalent patch capacitance, where $c_{s(\text{edge})}$ and $c_{p(\text{edge})}$ are the equivalent edge capacitances of feed strip and radiator patch, respectively.

As the feed strip is much smaller than the radiator patch, fringing capacitance from the edges (c_{sl}, c_s, and c_{sw}) may be considered for this current scenario which can be calculated from [24]. Optimization of separation gap (g) enhances the matching profile, which exhibits a capacitance of c_g. The square ring is considered as a loop element, which is replaced with a series LC circuit of equivalent inductance ($L_r(\text{outer})$) and capacitance ($C_{r(\text{outer})}$) value. The complete lumped circuit equivalent of the developed suspended ring antenna may be modeled by considering the geometry as a dual-ring structure. Inception of rectangular slots on the ring formulates two symmetrical rings, which may be analyzed as a two-loop structure of the radiating element [25, 26]. Each loop can be represented as a series LC circuit of equivalent inductance and capacitance value ($L_{r(\text{outer})}$ & $C_{r(\text{outer})}$, $L_{r(\text{inner})}$ & $C_{r(\text{inner})}$), shown in Figure 5. As has been studied, a non-copper region in between the copper rings raises capacitance, which introduces a capacitance c_{g1} along with edge capacitance ($c_{ro(\text{edge})}$ and $c_{ri(\text{edge})}$).

The equivalent input impedance (Z_{in}) of the shown lumped circuit can be effectively calculated by substituting the individual impedance caused by the corresponding element at each section. The impedance (Z) for each subsection is derived below in Equations (5)–(7).

$$Z_{\text{feed strip}} = \left[\left(\frac{1}{Zc_{sl}} + \frac{1}{Zc_s} + \frac{1}{Zc_{sw}}\right) + \frac{1}{Zc_{s(\text{edge})}}\right]^{-1} \tag{5}$$

In Equation (5), the first and second parts represent the impedance due to feed strip and impedance due to edge capacitance, respectively. Here the impedances due to c_{sl}, c_s, c_{sw}, $c_{s(\text{edge})}$ are denoted by Zc_{sl}, Zc_s, Zc_{sw}, $Zc_{s(\text{edge})}$, respectively.

$$Z_{gap} = \frac{1}{j\omega c_g} \tag{6}$$

$$Z_{patch} = \frac{Z_{ri1} \times Z_{ro}}{Z_{ri1} + Z_{ro}} \tag{7}$$

where,

$$Z_{ri} = \left[j\omega c_{ri(\text{edge})} + \frac{1}{Z_{\text{ring(inner)}}} \right]^{-1}$$

$$Z_{ro} = \left[j\omega c_{p(\text{edge})} + \frac{1}{Z_{\text{ring(outer)}}} + j\omega c_{ro(\text{edge})} \right]^{-1}$$

$$Z_{ri1} = Z_{ri} + \frac{1}{j\omega c_{g1}}$$

$$Z_{ring(\text{inner})} = j\omega L_{r(\text{inner})} + \frac{1}{j\omega c_{r(\text{inner})}}$$

$$Z_{\text{ring (outer)}} = j\omega L_{r(\text{outer})} + \frac{1}{j\omega c_{r(\text{outer})}}$$

The impedance due to the ring structure and its edge capacitance are presented and calculated as Z_{ri} for inner ring and Z_{ro} for outer ring. Z_{ri1} is the equivalent impedance caused by the inner ring and a separation gap in between the two rings, which is derived in the above section. The complete electrical model [Figure 5] of the proposed antenna is considered for calculating the reflection coefficient and presented in Figure 10.

3. ANALYSIS OF EXPERIMENTAL AND MEASURED RESULT

The discussed antenna structure is designed and optimized using Hyperlynx Electromagnetic Simulator (EM) simulation tool. The full wave simulation of the antenna module has been carried out, and the optimized results are observed. The return loss characteristics ($|S_{11}|$ plotted in Figure 6 demonstrates that the optimized square ring slot MPA shows multi-resonance characteristics where each band has a unique application in specific wireless technology as identified. Superior impedance bandwidth at each resonating frequency is observed with -10 dB reference, as demonstrated in the same figure. The band of operation allowed in the first resonance 3.4 GHz is 3.35–3.48 GHz, which is of 130 MHz. The second resonance 4.5 GHz allows operation between 4.38–4.74 GHz, which is around 360 MHz of bandwidth. The third resonance 5.8 GHz offers wideband operation of 850 MHz between 5.53 and 6.2 GHz. As a consequence, 380 MHz bandwidth is realized from 7.36 to 7.74 GHz at the fourth resonant frequency 7.5 GHz. Additionally, the operational bandwidth at each resonance is enhanced up to 12% by optimizing the parameters of the suggested microstrip antenna. With this description, the suggested multi-band antenna exhibits better performance at all RF bands discussed. However, as demonstrated in Figure 6 the narrow band difficulties of microstrip antennas is successfully conquered. Comparatively, all the resonant frequencies have a great application in Wi-MAX/Military fixed mobile communication/WLAN/ANS system, respectively. The operational bandwidth at each resonance is determined from the return loss characteristics as discussed in the above section and identified in the same plot presented in Figure 6. However, in this investigation improved band of operation is achieved at each resonant frequency which conquers the narrowband detriment of MPA.

The fundamental resonating modes of the developed suspended antenna may be calculated from [27]. The excitation due to TM_{mn} modes depends on the balanced point of the probe feed. In this scenario, the conventional antenna (Figure 1(b)) is designed to operate at TM_{10} mode. However, the dual-ring representation of the suspended slotted ring antenna exhibits different modes of propagation

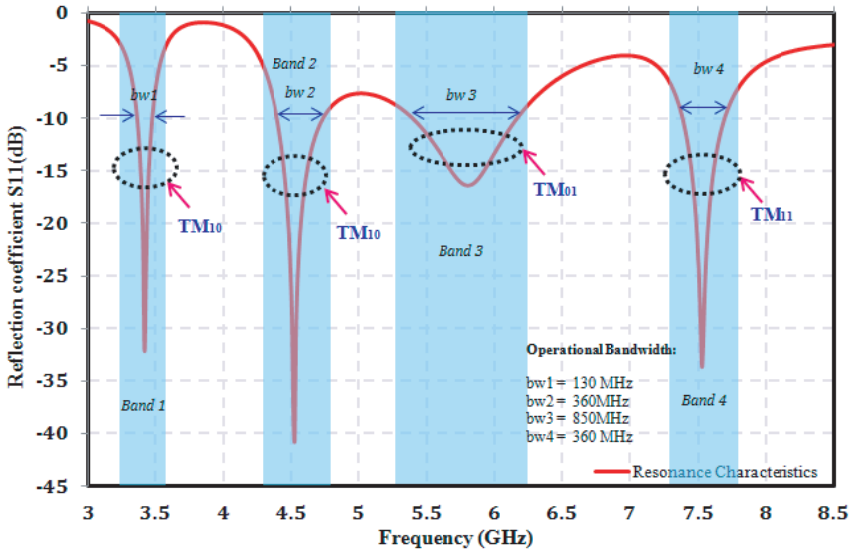

Figure 6. Operating band identification at each resonant frequency.

(Figure 6). In the developed structure, TM_{10} mode exists in lower order resonances (3.5 GHz and 4.5 GHz), TM_{01} mode in middle order resonances, and the antenna supports TM_{11} mode in the higher order resonance.

The single element radiator on the dielectric substrate is excited using EM coupling technique. For this a separate patch is introduced alongside the ring with a separation gap (g). Typically, in this design the matching characteristics and antenna performance depend on optimized 'g' value. Along with this, the width of the feed patch also influences the impedance matching while it has been observed that the influence due to the change in W_f is negligible. A parametric study has been presented in Table 2 by optimizing the coupling distance "g", and feed length "L_f". However, using $g = 0.5$ mm and $l_f = 0.8$ mm, good return loss characteristic is achieved as demonstrated in Figure 7.

As discussed, the antenna experiences better excitation as well as impedance matching using probe feeding technique. This statement can be well verified by analyzing the current distribution display by referring to the color palette shown in Figure 8. It has been observed that the suggested antenna patch has sufficient amount of current flow in the ring structure during the full-wave simulation and

Table 2. Step by step observation of the S_{11} response by optimizing the coupling distance "g", and "L_f".

Coupling Distance (g)	L_f	W_f	S_{11} Response			
			3.4 GHz	4.5 GHz	5.8 GHz	7.5 GHz
0.7	0.8	1.2	−26	−26	−15	−37
0.6	0.8	1.2	−33	−29	−15	−35
0.5	0.8	1.2	−41	−39	−16	−34
0.4	0.8	1.2	−28	−35	−17	−30
0.3	0.8	1.2	−23	−27	−18	−27
0.7	0.6	1.2	−28	−25	−15	−40
0.6	0.6	1.2	−34	−32	−15	−36
0.5	0.6	1.2	−32	−41	−16	−34
0.4	0.6	1.2	−26	−30	−17	−30
0.3	0.6	1.2	−21	−24	−18	−28

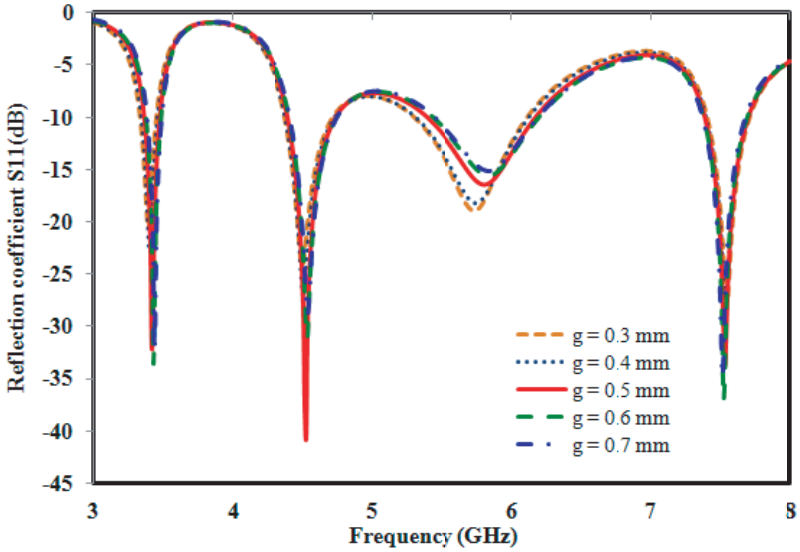

Figure 7. Optimization of S_{11} parameter by varying the coupling distance.

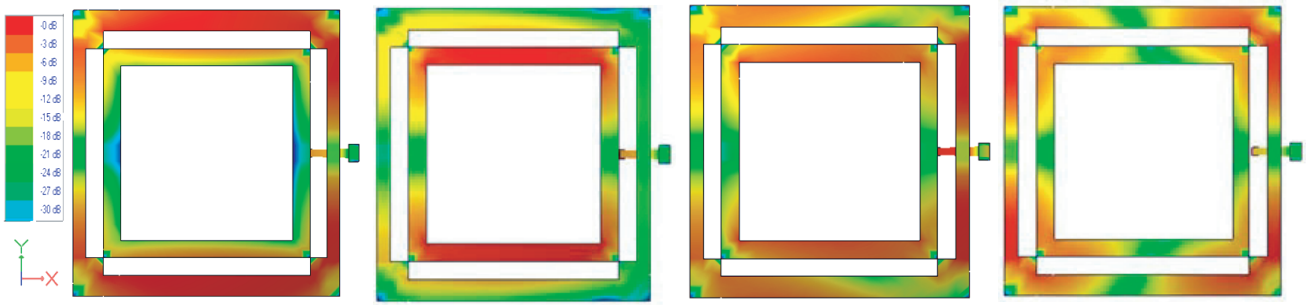

Figure 8. Current distributions at each operating band. (a) 3.5 GHz. (b) 4.5 GHz. (c) 5.8 GHz. (d) 7.5 GHz.

measurement process, wherein the red color represents the maximum current flow in the MPA as per MTT.

The suggested multi-band MPA was fabricated on an FR4 substrate as considered in the full wave simulation. The MPA was fabricated by adopting photolithography process, in which the antenna patch is implanted on the FR4 substrate, and a fully conducting copper plate was considered as the ground plane. Thereafter the radiator patch and ground plane are united with an air layer in between them, which gives in the ultimate architecture of the suggested multi-band antenna. The feeding section of the fabricated antenna was employed with a feed strip, feed probe followed by an SMA connector. The SMA connector is connected at the bottom surface of the conducting copper plate or the ground plane. The feed line is extended from the ground plane to the feed patch at the top layer present alongside the radiator patch. The inherent radiation from the feed probe may be avoided by using a teflon enclosure around the feed probe. The coaxial probe is connected to the SMA connector for giving the necessary signal intended for propagation.

A foam layer of dielectric constant ($\varepsilon_r = 1$) may be used in between the dielectric layer and the ground plane to evade the misalignment of the layers, which may cause deviation of the results. The fabricated images are exposed in Figure 9. The effective size of the antenna is comparable to a one rupee coin. The experimental and theoretical results and viable characteristics of the suggested antenna are discussed in the above section along with Figure 9.

(a) (b) (c)

Figure 9. Fabricated prototype of the suggested multi-band antenna. (a) Top view of the fabricated prototype. (b) Bottom-view of the fabricated prototype. (c) Side-view of the fabricated prototype.

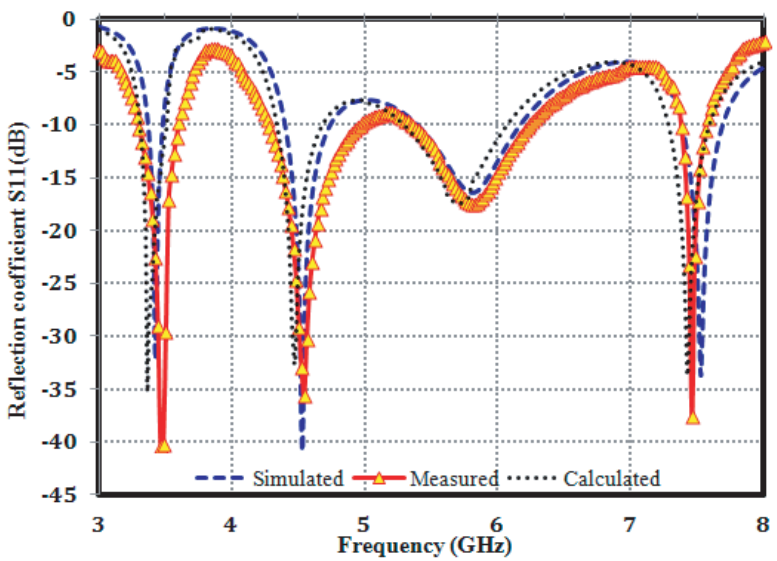

Figure 10. Measured Return loss characteristics ($|S_{11}|$ in comparison with simulated and calculated.

The fabricated prototype is taken into consideration for realizing the return loss characteristics using a vector network analyzer. Before the measurement process, the Agilent VNA (vector network analyzer) needs to be calibrated using a different load (short, open, and broadband) with the specified frequency range. It is very essential to calibrate the VNA with the operating range of the MPA in order to avoid error during the measurement process. Figure 10 displays the measured return loss characteristics extracted from the VNA. It has been observed that the measured $|S_{11}|$ agrees well with the simulated and calculated return loss. The fabricated MPA is then taken into the anechoic chamber for observing the radiation characteristics. Here the radiation pattern is measured in different angles (both $\emptyset$ & θ), and respective plots were recorded. The gain and directivity of the suggested antenna are measured by considering a horn antenna as a reference source. The chamber is fully calibrated as per specification. Usually the measured data (measured power) are in dBm, which need to be synchronized to dB power.

The radiation pattern of the suggested multi-band antenna is shown in Figure 11. The E-plane and H-plane patterns are observed. The radiation pattern of the suggested antenna is measured from different angles in the anechoic chamber. Both E-plane and H-plane radiation characteristics of the fabricated antenna were observed with 5° step angle. The measured patterns are plotted at right-hand side along with the IE3D simulated pattern at the left-hand side. It has been observed that

the simulated patterns have good agreements with the measured pattern in the foresight direction. The corresponding E co-pol and H co-pol patterns are near 0 dB, which is one of the norms that the antenna should meet for having better polarization characteristics. The E cross-pol and H cross-pol patterns are marked in dashed lines for respective resonances. It has been observed that the simulated patterns have good agreement with the measured pattern in the broadside direction. However, better radiation characteristics are analyzed from the measured pattern exposed in Figure 11. Although the back radiation of the measured E-co and H-co pattern is less than the radiation in broadside direction, the antenna shows good radiation characteristics as required.

The experimental results of the fabricated antenna are presented in Table 3. The average boresight gain of the suggested antenna is well above 6 dBi. Despite that, the antenna realizes a good VSWR

Table 3. Experimental results of the suspended multi-resonance antenna.

Resonant Frequency	S_{11} Result		Gain Response (dB)	
	Simulated	Measured	Simulated	Measured
3.5 GHz	−32	−40	6.3	6.5
4.5 GHz	−41	−36	5.2	5.2
5.8 GHz	−17	−184	6.4	6.45
7.5 GHz	−34	−37	5	5.16

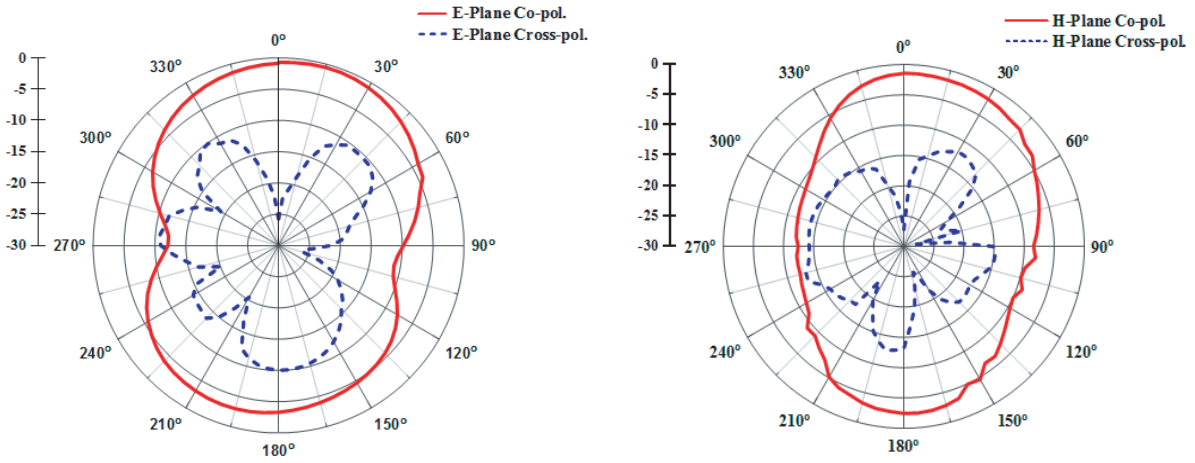

(a)

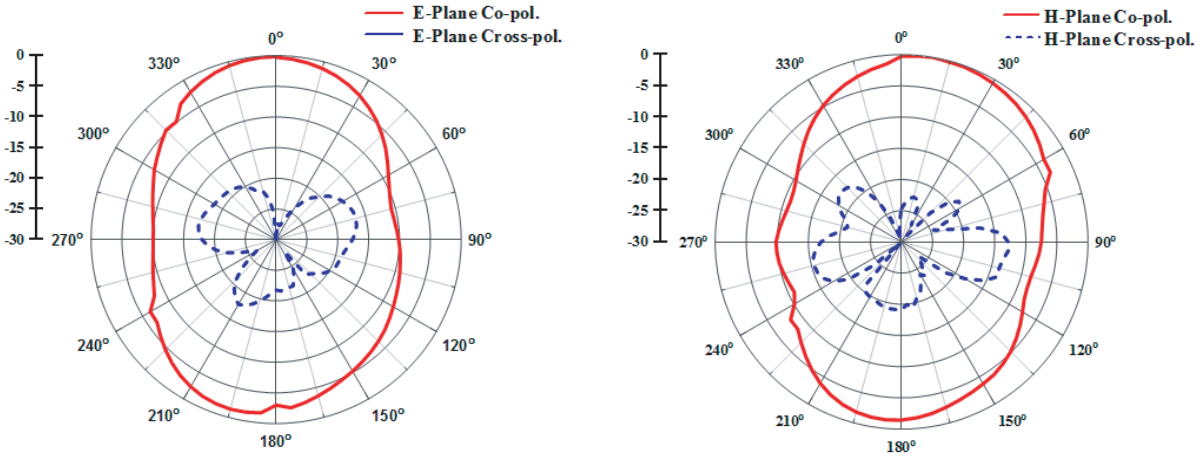

(b)

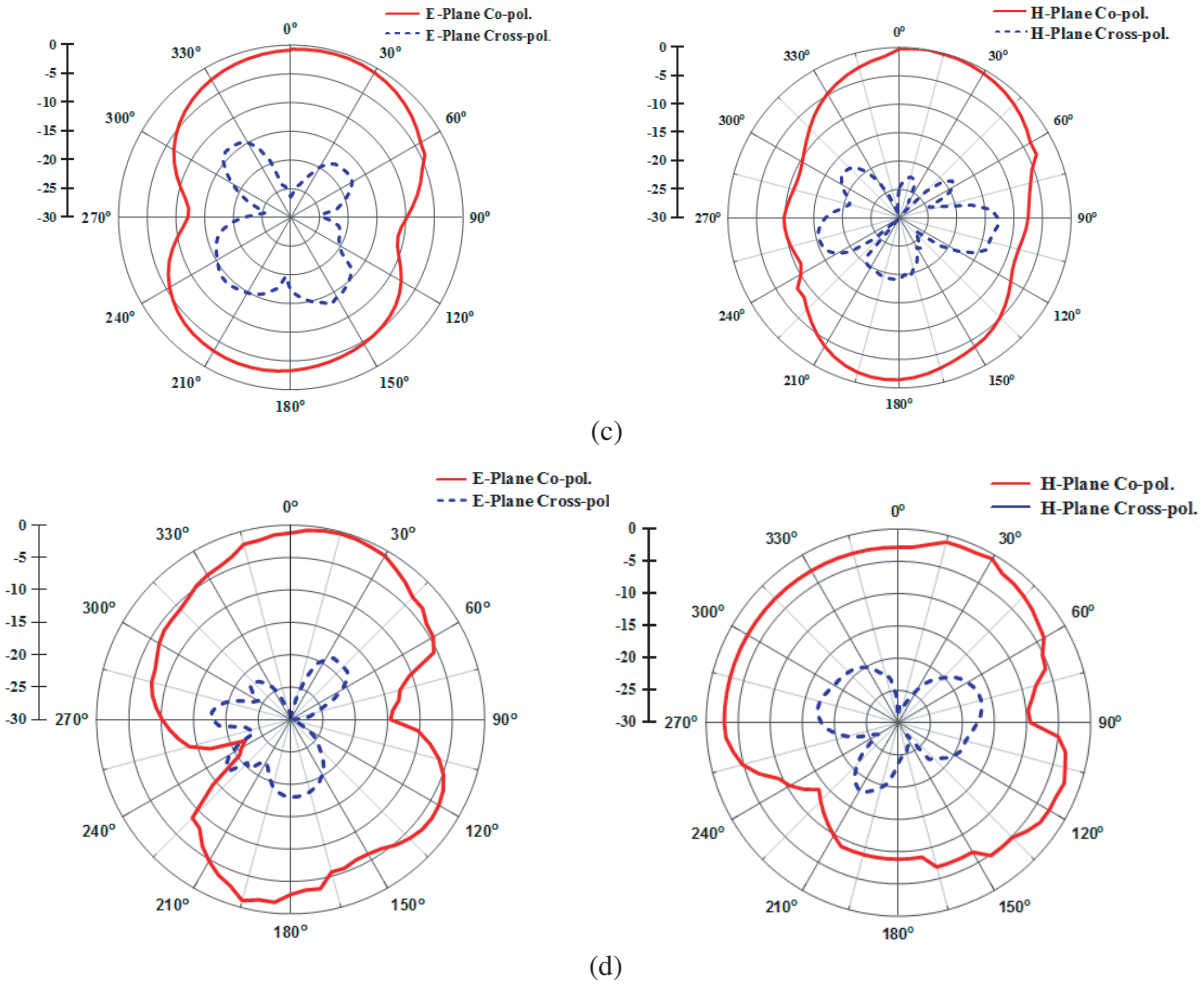

Figure 11. The Radiation pattern of the suggested suspended MPA at each resonant frequency. (a) 3.5 GHz. (b) 4.5 GHz. (c) 5.8 GHz. (d) 7.5 GHz.

of well below 2 and average efficiency of 93% at each resonating frequency. It has been observed that the fabricated antenna has better matching characteristics. Without any misalignment, there is a good agreement between the simulated, calculated and measured results. However, owning to all these novel characteristics the antenna is suggested for multi-standard multi-functional modern wireless communication.

4. CONCLUSION

In this paper, a novel compact slotted ring structure is investigated for multi-resonance operation. The designed methodology follows the multi-layer structure, wherein electromagnetic coupling is considered for excitation purpose. The slots in the ring structure yields quad-band operation with improved polarization characteristics and enhances the gain response up to 6 dBi. The developed suspended slotted ring antenna is inspired with different resonating modes such as TM_{10}, TM_{01}, and TM_{11}. The suggested MPA finds its notable application in modern wireless technology such as Wi-MAX/Military fixed mobile communication/WLAN/ANS system, respectively, along with the below 6 GHz 5G mobile communication systems and configuration of IoTs. The operational bandwidth at each resonant frequency is enhanced up to 12%, which is achieved by maintaining the optimized layer gap between the antenna patch and the ground plane. The suggested antenna structure was fabricated and measured for

validating the antenna characteristics. Here, quad-band resonance can be achieved through single port analysis instead of multi-port analysis, which is a major advantage of this structure, thus reduces the system complexity and cost, minimizes the number of base stations, supports multi-tasking environment, and reduces the size of the communication device, etc. Owning to these novel characteristics, the MPA is suggested for multi-standard wireless communication system like IEEE 802.16, IEEE 802.11, etc. This design has a novel application in next generation multi-tasking IoTs and WSNs.

ACKNOWLEDGMENT

This research is supported by Science and Engineering Research Board, Govt. of India (DST-SERB). Infrastructure is given by the school of Electronics Engineering, KIIT University, Odisha. The author would like to thank Dr. Vivek Singh for giving lab support in testing and measuring the MPA and Seshadri binaya Behera for technical English writing.

REFERENCES

1. Costantine, J., K. Y. Kabalan, A. Ei-Hajj, and M. Rammal, "New multi-band microstrip antenna design for wireless communications," *IEEE Antennas and Propagation Magazine*, Vol. 49, No. 6, 2007.
2. Jiang, F., J. Chen, Swindlehurst, A. Lee, and J. A. Lopez-salcedo, "Massive MIMO for wireless sensing with a coherent multiple access channel," *IEEE Transactions on Signal Processing*, Vol. 63, No. 12, June 2015.
3. Park, D.-H. and Y.-S. Kwak, "Design multi-band microstrip patch antenna for wireless terminals," *IEEE Future Generation Communication and Networking Letter*, Vol. 2, 439–441, 2007.
4. Sharawi, M. S., "Printed multi-band MIMO antenaa systems and their performance metrics," *IEEE Antennas and Propagation Magazine*, Vol. 55, No. 5, 2013.
5. Balanis, A., *Antenna Theory Analysis and Design*, 3rd Edition, A John Wiley & Sons, Inc Publication, 2003.
6. Liao, W., S. Chang, and L. Li, "A compact planer multiband antenna for integrated mobile devices," *Progress In Electromagnetic Research*, Vol. 109, 1—16, 2010.
7. Fallahpour, M., M. T. Ghasr, and R. Zoughi, "Miniaturized reconfigurable multiband antenna for multiradio wireless communication," *IEEE Transactions on Antennas and Propagation*, Vol. 62, No. 12, 6049–6059, 2014.
8. Wang, C. and S.-W. Chang, "Studies on dual-band multi-slot antennas," *Progress In Electromagnetic Research*, Vol. 83, 293–306, 2008.
9. Sarkar, D., K. Saurav, and K. V. Srivastava, "Multi-band microstrip-fed slot antenna loaded with split-ring resonator," *IET Electronics Letters*, Vol. 50, No. 21, 1498–1500, 2014.
10. Kokotoff, D. M., J. T. Aberle, and R. B. Waterhouse, "Rigorous analysis of probe-fed printed annular ring antennas," *IEEE Transactions on Antennas and Propagation*, Vol. 47, No. 2, 384–388, 1999.
11. Akyildiz, I. F., W. Su, Y. Sankarasubramaniam, and E. Carirci, "Wireless sensor networks: A Survey," *ELSEVIER Journal on Computer Networks*, Vol. 38, No. 4, 393–442, 2002.
12. Lei, Y., Y. Zhang, and Y. Zhao, "The research of coverage problems in wireless sensor network," *IEEE WINS Proceedings*, 31–34, 2009, ISBN: 978-0-7695-3901-0.
13. Nassar, I. T., J. Wang, J. L. Frolik, and T. M. Weller, "A high-efficiency, miniaturized sensor node with 3-D machined-substarte antennas for embedded wireless monitoring," *IEEE Sensors Journal*, Vol. 15, No. 9, 5036–5044, September 2015.
14. Agiwal, M., A. Roy, and N. Saxena, "Next generation 5G wireless networks: A comprehensive survey," *IEEE Communications Surveys & Tutorials*, Vol. 18, No. 3, 1617–1655, 2016.
15. Internet of Things: Wireless Sensor Networks, Iternational Electrotechnical Commission, Geneva, Switzerland, 2014.

16. Yurduseven, O., D. Smith, N. Pearsall, and I. Forbes, "A solar cell stacked slot-loaded suspended microstrip patch antenna with multi-band resonance characteristics for WLAN and WIMAX systems," *Progress In Electromagnetics Research*, Vol. 142, 321–332, 2013.
17. "Optimizing 4 GHz mission critical networks," *Microwave Journal*, Billerica, MA, 2009.
18. Youell, T., "NTT Docomo and Nokia research 5G in 4.4–4.9 GHz bands," Policy Tracker, July 2015.
19. http//www.policytracker.com/headlines/ntt-docomo-and-nokia-research-5g-in-4.4-2013-4.9-ghz-band.
20. Behera, S. and D. Barad, "Design of microstrip antenna for wireless communication with compact size," *IEEE ICECCT Proceedings*, Vol. 3, 1473–1476, 2015, ISBN: 978-1-4799-6085-9.
21. Behera, S. and D. Barad, "A novel design of microstrip fractal antenna for wireless sensor network," *IEEE ICCPEIC Proceedings*, 2015, ISBN: 978-1-4673-6524-6.
22. Behera, S. and K. J. Vinoy, "Microstrip square ring antennas for dual-band operation," *Progress In Electromagnetics Research*, Vol. 93, 41–56, 2009.
23. Behera, S. and D. Barad, "Circular polarized dual-band antenna for WLAN/Wi-MAX application," *Int. J. RF and Microwave Comp. Aid. Eng.*, 2016, doi:10.1002/mmce.21046.
24. Kasabegoudar, V. G. and K. J. Vinoy, "Coplaner capacitive coupled probe fed microstrip antennas for aideband applications," *IEEE Transactions on Antennas and Propagation*, Vol. 58, No. 10, 3131–3138, 2010.
25. Chang, K. and L. Hsieh, *Microwave Ring Circuits and Related Structures*, 2nd Edition, Chapter 1, John Wiley & Sons, Inc Publication, USA, 2004.
26. Stutzmanet, W. L., et al., *Antenna Theory and Design*, 3rd Edition, John Wiley & Sons, Inc Publication, USA, 2013.
27. Guha, D. and Y. M. N. Antar, *Microstrip and Printed Antennas New Trends Techniques & Application*, 2nd Edition, Chapter 2, John Wiley & Sons, Inc Publication, UK, 2011.